

Original paper

Quantitative CT texture analysis of the mandibular condyle in medication-related osteonecrosis of the jaw

Naoya Nakamura^{1,A,B,C,D,E,F}, Hirotaka Muraoka^{2,C,E}, Satoshi Tokunaga^{2,D}, Kohei Otsuka^{2,C}, Tomohiro Komatsu^{2,A}, Hitomi Kishimoto^{1,B}, Sawa Muranaka^{1,B}, Kotaro Ito^{2,B,D}

¹Nihon University Graduate School of Dentistry at Matsudo, Matsudo, Japan

²Nihon University-Matsudo Campus, Matsudo, Japan

Abstract

Purpose: In this study, we quantitatively assessed the involvement of the mandibular condyle in patients with medication-related osteonecrosis of the jaw (MRONJ) based on computed tomography (CT) texture analysis.

Material and methods: We analyzed CT scans obtained between April 2020 and March 2023, from 31 patients (7 males and 24 females) with MRONJ. We extracted 279 radiomic features from regions of interest defined on the affected and control sides. These features were analyzed using MaZda version 4.6.2.0. Using Fisher's coefficient, 10 of these features were selected for analysis. The selected features were compared between the affected and control sides using the paired *t*-test and the Wilcoxon signed-rank test. Significance was set at $p < 0.05$.

Results: All selected radiomics features, which were texture features of the mandibular condylar bone marrow, showed significant differences between the affected and control sides in patients with MRONJ ($p < 0.05$).

Conclusions: These findings suggested that microstructural changes, not easily detected on visual inspection, may occur in the trabecular structure of the affected mandibular condyle in patients with MRONJ. Therefore, the impact of the disease on the temporomandibular joint should be considered in MRONJ.

Key words: computed tomography, mandibular condyle, medication-related osteonecrosis of the jaw, texture analysis.

Introduction

Antiresorptive agents are commonly used to treat multiple myeloma, bone metastases from solid tumors, and osteoporosis. These drugs inhibit osteoclast activity and reduce bone resorption throughout the skeleton, including that in the jawbone [1-3].

The condition was initially termed bisphosphonate-related osteonecrosis of the jaw when it was first reported as a serious adverse event in 2003 [1,4]. However, subsequent cases were linked to the use of antiangiogenic agents and tyrosine kinase inhibitors, leading to adoption of the broader term medication-related osteonecrosis of the jaw (MRONJ),

which was defined by the American Association of Oral and Maxillofacial Surgeons in its 2022 position paper [1]. MRONJ is characterized by the presence of exposed bone or bone that can be probed through a fistula in the maxillofacial region, which persists for more than 8 weeks in patients who have been treated with a bone-modifying or antiangiogenic agent, and who have no history of radiation therapy or metastatic disease involving the jaw.

Computed tomography (CT), panoramic radiography, and magnetic resonance imaging (MRI) are effective imaging modalities for diagnosing MRONJ [5]. Among these, CT is particularly valuable for the three-dimensional assessment of changes in bone, such as osteosclerosis, cortical bone

Correspondence address:

Naoya Nakamura, Nihon University Graduate School of Dentistry at Matsudo, 2-870-1 Sakaecho-Nishi, Matsudo, Chiba 271-8587 Japan,
e-mail: mana25012@g.nihon-u.ac.jp

Authors' contribution:

A Study design · B Data collection · C Statistical analysis · D Data interpretation · E Manuscript preparation · F Literature search · G Funds collection

destruction, and sequestrum formation, as well as the associated complications [6]. Although abnormalities with well-defined structural features can be readily identified by visual inspection, evaluation of the more complex patterns commonly encountered in medical imaging remains challenging and requires advanced diagnostic expertise. In this context, texture analysis is an emerging quantitative imaging analysis technique that can facilitate the detection of subtle structural alterations by extracting numerous statistically derived features from medical images [7].

MRONJ can significantly affect areas beyond the primary lesion, including the development of pathological fractures and spread of inflammation to the surrounding tissues [8-10]. Therefore, a comprehensive and detailed evaluation is clinically important. The mandibular condyles of patients with MRONJ have been examined using cone-beam CT or MRI in several previous studies [11,12]. However, to the best of our knowledge, no study has evaluated the mandibular condyles in patients with MRONJ using texture analysis of CT images.

In order to gain further insight into the involvement of the mandibular condyle in cases of MRONJ, we here evaluated the mandibular condyles of patients with MRONJ quantitatively using texture analysis of CT images. The null hypothesis was that MRONJ would not affect the mandibular condyle.

Material and methods

Study design and patients

This retrospective study was approved by our institutional review board, and the requirement for informed consent

was waived (No. EC25-23-002-1). This study included patients who underwent CT for suspected MRONJ between April 2020 and March 2023 at the outpatient clinic of our university hospital. Among these, patients with MRONJ affecting only one side of the mandible (7 men and 24 women; age range: 65-95 years; mean age: 80 years; 62 temporomandibular joints) were selected for analysis. For these patients, the control side was confirmed to show no sclerotic changes on CT and no abnormal signal intensity on MRI.

We excluded patients in whom the effects of MRONJ extended across the midline to the control side; patients with a history of radiotherapy; patients with conditions that could affect the mandibular condyle or bone marrow, such as cystic lesions, tumors, malignancies, hematologic disorders, anemia, diabetes mellitus, rheumatoid arthritis, or malnutrition; and patients suspected of having temporomandibular joint osteoarthritis.

Image acquisition

CT was performed using a 64-slice multidetector CT system (Aquilion 64; Toshiba Medical Systems, Tokyo, Japan) according to the standard clinical protocol for craniofacial imaging at our institution. The imaging parameters used were as follows: tube voltage of 120 kV, tube current of 100 mA, field-of-view of 240 mm × 240 mm, and helical pitch of 41. Imaging was performed using axial images of 0.50-mm thickness. The CT images were viewed on a medical-grade liquid crystal display monitor (RadiForce G31, Eizo Nanao, Ishikawa, Japan).

Using axial slices showing the maximal cross-sectional areas of both mandibular condyles, an oral radiology specialist with 12 years of experience manually traced regions

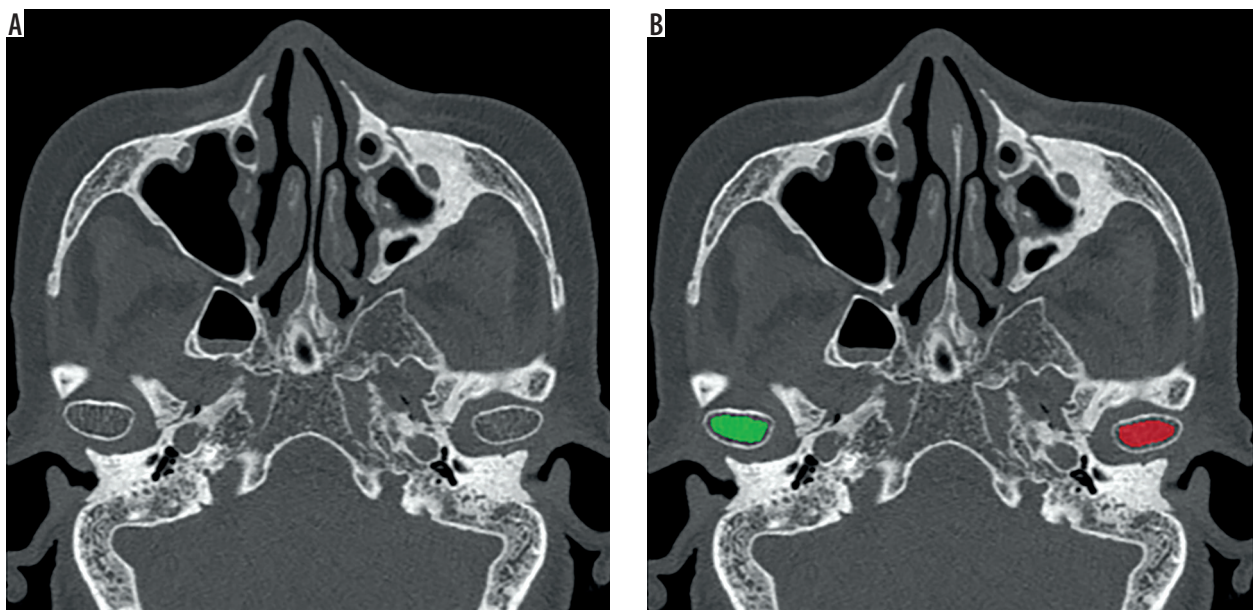


Figure 1. In patients with medication-related osteonecrosis of the jaw (MRONJ), a region of interest (ROI) was manually drawn on computed tomography (CT) images to encompass the maximum measurable area on both sides. Axial CT image of the patient with MRONJ before (A) and after (B) ROI delineation. The ROI on the affected side is shown in red, while the ROI on the control side is shown in green

Feature name	V-1	V-2	Feature name	V-1	V-2	Feature name	V-1	V-2	Feature name	V-1	V-2	Feature name	V-1	V-2
Area	2193	2382	Area_S11_1	4106	4504	Area_S12_1	3932	4406	Area_S13_1	3796	4230	Area_S14_1	3602	4058
Mean	94.52	91.58	S11_1ConEnt	0.02126	0.02124	S12_1ConEnt	0.02095	0.02122	S13_1ConEnt	0.01854	0.01943	S14_1ConEnt	0.01815	0.01915
StdDev	0.32607	0.34689	S11_1ConEne	0.84121	0.79502	S12_1ConEne	0.52981	0.41596	S13_1ConEne	0.24816	0.02695	S14_1ConEne	0.06955	0.02621
Skewness	0.07505	0.34048	S11_1ConMom	0.95566	0.56277	S12_1ConMom	0.42373	0.40542	S13_1ConMom	0.25684	0.30359	S14_1ConMom	0.325	0.37131
Kurtosis	77	73	S11_1ConSur	48.079	46.281	S12_1ConSur	48.079	46.413	S13_1ConSur	48.119	46.421	S14_1ConSur	48.133	46.412
Area_S11_2	4312	4680	S11_2ConEnt	0.02022	0.02021	S12_2ConEnt	0.02027	0.02025	S13_2ConEnt	0.02027	0.02025	S14_2ConEnt	0.02027	0.02025
Area_S11_3	4102	4504	S11_3ConEnt	0.02151	0.02151	S12_3ConEnt	0.02151	0.02151	S13_3ConEnt	0.02151	0.02151	S14_3ConEnt	0.02151	0.02151
Area_S11_4	4220	4566	S11_4ConEnt	0.02151	0.02151	S12_4ConEnt	0.02151	0.02151	S13_4ConEnt	0.02151	0.02151	S14_4ConEnt	0.02151	0.02151

Figure 2. Among all extracted features, the ten features with the highest Fisher coefficients were selected

of interest (ROIs) in the condyles on both sides to delineate the bone marrow. Structures that could potentially affect the image, such as the cortical bone, were excluded from the ROIs (Figure 1).

Texture features of the mandibular condyles on the affected and control sides of patients with MRONJ were analyzed using the open-access software MaZda version 4.6.2.0 (Institute of Electronics, Technical University of Lodz, Poland) [13–15]. To use this software, DICOM images were first converted into bitmap (BMP) format. Using CT settings for bone tissue (window level: 500 Hounsfield units [HU]; window width: 2800 HU), 279 texture features were extracted from each ROI in single-slice CT images. The images were normalized using the MaZda default (the intensity range of the image under analysis, from 1 to Ng = 2 k, where k is the number of bits per pixel used to encode the image under analysis). The parameters for extracting the features were as follows: gray-level run length matrix (GLRLM), 6 bits/pixel, 4 di-

rections (0°, 45°, 90°, 135°); gray-level co-occurrence matrix (GLCM), 6 bits/pixel, 4 directions (0°, 45°, 90°, 135°), 5 distances (n = 1, 2, 3, 4, 5), absolute gradient; 4 bits/pixel, wavelets 8 bits/pixel. The texture features for each group (control and MRONJ) were selected based on their Fisher coefficients (Figure 2, Table 1), which represent the ratio of the between-class variance to the within-class variance and tends to increase when the correlation between features decreases. Further details on parameter selection are available on the software package website (<http://www.eletp.lodz.pl/programy/mazda>).

Variables

In this study, the primary predictor variable was the presence or absence of mandibular condyle involvement. The outcome variables were the texture features extracted from the ROIs on CT images, including histogram, GLCM, GLRLM, autoregressive model, and wavelet transform features.

Table 1. Texture features extracted in the analysis

Feature class	Description
Histogram	
Percentile	The intensity of pixels on the image, without any spatial relations
GLCM	
Correlat	The linear dependency between the gray levels It is low for low linear dependency and high for high linear dependency
SumEntp	An index that evaluates the variation in the sum of gray-level intensities of adjacent pixels
Autoregressive model	
Sigma	The extent of variation in image information (noise) not captured by the autoregressive model
Wavelet transform	
WavEnLL	An index evaluating image smoothness and coarse intensity patterns based on the energy of the low-frequency (LL) component from wavelet transformation

Correlat – correlation, GLCM – gray-level co-occurrence matrix, SumEntp – sum entropy, WavEnLL – wavelet energy of the LL subband

Table 2. Texture features of mandibular condyle bone marrow differentiating between the presence and absence of medication-related osteonecrosis of the jaw (MRONJ)

Variable	Control side (n = 31)	MRONJ side (n = 31)	Fisher coefficient	p-value
Age (years) ±SD	80 ± 5.4	80 ± 5.4		
Sex				
Male (n = 14)	7	7		
Female (n = 48)	24	24		
Histogram				
Percentile 90 ±SD	105.55 ± 8.15	115.06 ± 9.72	1.1630	< 0.001*
Percentile 99 ±SD	118.84 ± 10.89	132.03 ± 12.99	1.2521	< 0.001*
GLCM				
S(0,1)Correlat [IQR]	0.91 [0.89-0.92]	0.92 [0.92-0.93]	1.1802	< 0.001**
S(0,2)Correlat ±SD	0.71 ± 0.06	0.76 ± 0.05	1.1332	< 0.001*
S(1,1)Correlat ±SD	0.82 ± 0.03	0.85 ± 0.03	1.4633	< 0.001*
S(2,2)Correlat ±SD	0.48 ± 0.09	0.58 ± 0.09	1.2297	< 0.001*
S(3,3)SumEntrp ±SD	1.21 ± 0.11	1.31 ± 0.09	1.0891	< 0.001*
S(4,0)SumEntrp ±SD	1.22 ± 0.1	1.32 ± 0.09	1.1129	< 0.001*
Autoregressive model				
Sigma ±SD	0.17 ± 0.02	0.15 ± 0.02	1.0756	< 0.001*
Wavelet transform				
WavEnLL_s-2 ±SD	8383.32 ± 1039.46	9630.07 ± 1372.68	1.0835	< 0.001*

*Paired *t*-test. **Wilcoxon signed-rank test.

Correlat – correlation, GLCM – gray-level co-occurrence matrix, IQR – interquartile range, SD – standard deviation, SumEntrp – sum entropy, WavEnLL – wavelet energy of the low-frequency subband

Statistical analysis

The paired *t*-test and the Wilcoxon signed-rank test were used to compare texture features between the two groups. The normality of distribution of each texture feature was assessed using the Shapiro-Wilk test. SPSS software for Windows (IBM Corp., Armonk, NY, USA) was used for all analyses. A *p*-value of less than 0.05 was considered statistically significant. Post-hoc statistical power analysis was performed using G*Power 3.1.9.2 (Heinrich Heine University, Düsseldorf, Germany).

Results

Table 2 presents diagnostic and demographic data (age and sex) of the patients, and a summary of CT texture features. The mean age of patients with MRONJ was 80 ± 5.4 years (*n* = 31).

The top-10 texture features selected from the overall 279 features extracted by CT texture analysis were as follows: two histogram features (90th percentile, 99th percentile), six GLCM features (S(0,1)Correlation, S(0,2)Correlation, S(1,1)Correlation, S(2,2)Correlation, S(3,3)Sum Entropy, S(4,0)Sum Entropy), one autoregressive model feature (Sigma), and one wavelet-transform feature (Wavelet Energy in the Low-Low subband_s-2). These texture features were significantly more common on

the affected side than on the control side in patients with MRONJ (*p* < 0.001) (Figures 3 and 4).

The *post-hoc* power analysis demonstrated that the achieved statistical power ranged from 0.9995 to 0.9999.

Discussion

In this study, texture features of the mandibular condylar bone marrow on CT images exhibited significant differences between the affected and control sides of patients with MRONJ.

In texture analysis, a histogram is a statistical representation of the distribution of gray levels within a ROI and serves as a fundamental parameter for the quantitative evaluation of image brightness and contrast. The 90th percentile represents the maximum gray level after excluding the top 10% of the high-intensity pixels from the distribution of pixel gray levels. This serves as a representative measure of the high-intensity range, and minimizes the influence of outliers and extreme values. Similarly, the 99th percentile represents the maximum gray level after excluding the top 1% of the high-intensity pixels from the distribution of the pixel gray levels. In this study, both the 90th and 99th percentiles were higher on the affected side than on the control side in the mandibular condyles of patients with MRONJ, indicating elevated gray levels within the bone marrow on the affected side.

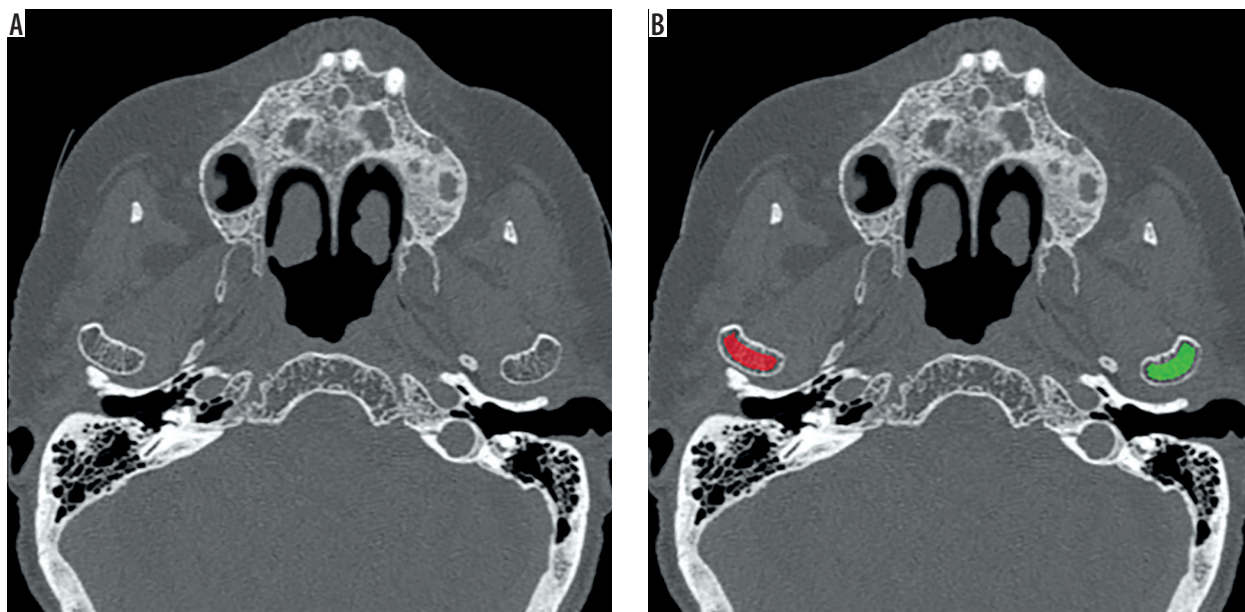


Figure 3. The patient was a 95-year-old female with medication-related osteonecrosis of the jaw (MRONJ) of the right mandible. Axial computed tomography images of the patient with MRONJ before (A) and after (B) region-of-interest delineation

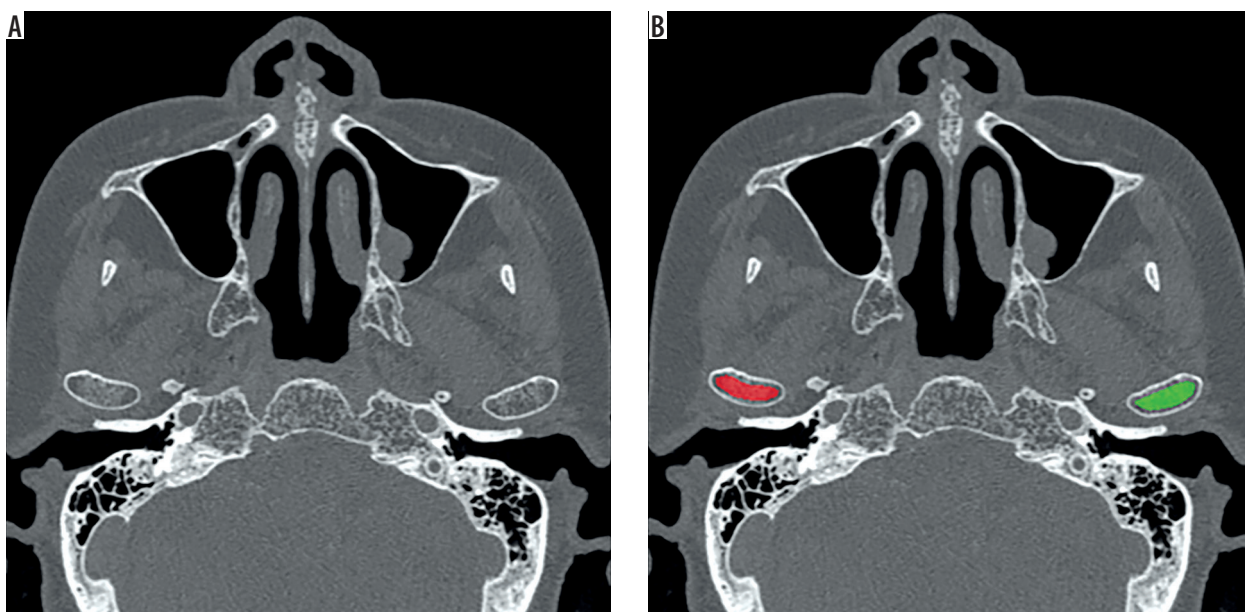


Figure 4. The patient was an 82-year-old female with medication-related osteonecrosis of the jaw (MRONJ) of the right mandible. Axial computed tomography images of the patient with MRONJ before (A) and after (B) region-of-interest delineation

The GLCM quantifies the texture regularity and complexity by recording the frequency of gray-level combinations between neighboring pixels. Correlation measures the similarity between neighboring gray levels, with higher values indicating stronger directional patterns, whereas Sum Entropy reflects the complexity of gray-level sums, with higher values indicating greater variability. In this study, both the Correlation and Sum Entropy were significantly higher on the affected side than on the control side in patients with MRONJ. This suggests localized directional patterns and increased structural heterogeneity in the trabecular architecture of the mandibular condyle.

The autoregressive model predicts pixel values based on surrounding pixels, with Sigma representing unexplained noise. The lower Sigma values on the affected side in this study indicated the presence of more predictable large-scale intensity patterns on this side than on the control side.

Wavelet transform decomposes an image into frequency components, while Wavelet Energy in the Low-Low subband reflects the contribution of the low-frequency patterns. Higher values on the affected side in this study suggested the presence of more prominent large-scale structures in the mandibular condyles of this side in patients with MRONJ.

These findings suggested that subtle changes that are difficult to detect with the naked eye may occur in the trabecular structure of the affected mandibular condyle in patients with MRONJ. Previously, Knoepflin *et al.* [16] reported that texture parameters, such as Sum Entropy and Correlation, reflect alterations in bone microarchitecture. Several studies have used texture analysis to evaluate subtle changes in bone structure [17-22]. Furthermore, Hirahara *et al.* [12] demonstrated that MRONJ cases showed significantly higher signal intensity in the bone marrow of the mandibular condyle on the symptomatic side on MRI. Additionally, previous reports have shown that osteomyelitis has widespread effects, including on the soft tissue [23-28]. Therefore, structural changes may occur in the bone microstructure of the affected temporomandibular joint region in patients with MRONJ, even in the absence of clinical symptoms in the temporomandibular joint. Consequently, imaging analysis may be particularly useful for early detection of lesion extension in patients with MRONJ. Not only does the affected area require attention, but evaluation and continuous management of the temporomandibular joint are also important.

This study had some limitations, including its retrospective design and the potential for selection bias, which could not be entirely avoided despite the strict criteria employed.

Conclusions

The CT texture characteristics of the mandibular condylar bone marrow demonstrated significant differences between the affected and control sides in patients with MRONJ, suggesting that bone microstructural changes may occur in the affected temporomandibular joint region even in the absence of clinical symptoms. Therefore, the effects of the condition on the temporomandibular joint in these patients should be considered.

Disclosures

1. Institutional review board statement: This retrospective study was approved by the Nihon University Ethics Committee (approval number EC25-23-002-1) and conducted in accordance with the Declaration of Helsinki.
2. Informed consent statement: The requirement for informed consent was waived due to the retrospective nature of the study.
3. Assistance with the article: None.
4. Financial support and sponsorship: None.
5. Conflicts of interest: None.

References

1. Ruggiero SL, Dodson TB, Aghaloo T, Carlson ER, Ward BB, Kademani D. American Association of Oral and Maxillofacial Surgeons' position paper on medication-related osteonecrosis of the jaws – 2022 update. *J Oral Maxillofac Surg* 2022; 80: 920-943.
2. Jensen PR, Andersen TL, Chavassieux P, Roux JP, Delaisse JM. Bisphosphonates impair the onset of bone formation at remodeling sites. *Bone* 2021; 145: 115850. DOI: 10.1016/j.bone.2021.115850.
3. Taguchi A, Shiraki M, Morrison A, Khan AA. Antiresorptive agent-related osteonecrosis of the jaw in osteoporosis patients from Asian countries. *Osteoporos Sarcopenia* 2017; 3: 64-74.
4. Marx RE. Pamidronate (Aredia) and zoledronate (Zometa) induced avascular necrosis of the jaws: a growing epidemic. *J Oral Maxillofac Surg* 2003; 61: 1115-1117.
5. Wongratwanich P, Shimabukuro K, Konishi M, Nagasaki T, Ohtsuka M, Suei Y, et al. Do various imaging modalities provide potential early detection and diagnosis of medication-related osteonecrosis of the jaw? A review. *Dentomaxillofac Radiol* 2021; 50: 20200417. DOI: 10.1259/dmfr.20200417.
6. Hoefert S, Schmitz I, Tannapfel A, Eufinger H. Importance of microcracks in etiology of bisphosphonate-related osteonecrosis of the jaw: a possible pathogenetic model of symptomatic and non-symptomatic osteonecrosis of the jaw based on scanning electron microscopy findings. *Clin Oral Investig* 2010; 14: 271-284.
7. Castellano G, Bonilha L, Li LM, Cendes F. Texture analysis of medical images. *Clin Radiol* 2004; 59: 1061-1069.
8. Tshako K, Sekido K, Ando T, Okita M, Harada M, Hariya Y. A case of successful treatment of medication-related osteonecrosis of the jaw with conservative treatment for pathological mandibular fracture. *Int J Surg Case Rep* 2024; 120: 109822. DOI: 10.1016/j.ijscr.2024.109822.
9. Yamashiro K, Sato A, Okazaki F, Nakano M, Sawaki K, Hirata Y, et al. Medication-related osteonecrosis of the jaws caused lethal sepsis in an edentulous patient with multiple systemic factors. *Clin Case Rep* 2016; 5: 97-103.
10. Suzuki T, Sekiya R, Hamada Y, Takahashi M, Karakida K, Sakamoto H. Fatal bleeding in conjunction with mandibular medication-related osteonecrosis of the jaw (MRONJ). *Bull Tokyo Dent Coll* 2018; 59: 27-34.
11. Sancar BS, Gök RŞ, Tunç S. Evaluation of the effects of bisphosphonate therapy on the temporomandibular joint using cone beam computed tomography. *Oral Radiol* 2025; 41: 430-437.
12. Hirahara N, Muraoka H, Noda M, Muramatsu T, Tokunaga S, Kaneda T. Change in the magnetic resonance imaging signal of the mandibular condyle due to bisphosphonate-related osteonecrosis of the jaw. *J Hard Tissue Biol* 2017; 26: 161-168.
13. Shin JW, Yoon S, Min BJ, Park DS. A novel copyright protection for digital images using the gradient of image intensity. In: *Proceedings of the 2007 International Symposium on Information Technology Convergence (ISITC 2007)*; 2007; Jeonju, South Korea, p. 227-234.

14. Szczypiński PM, Strzelecki M, Materka A, Klepaczko A. MaZda – a software package for image texture analysis. *Comput Methods Programs Biomed* 2009; 94: 66-76.
15. Strzelecki M, Szczypiński P, Materka A, Klepaczko A. A software tool for automatic classification and segmentation of 2D/3D medical images. *Nucl Instrum Methods Phys Res A* 2013; 702: 137-140.
16. Knoepflin P, Pithioux M, Bendahan D, Poullain F, Le Corroller T, Fabre C, et al. Texture parameters measured by UHF-MRI and CT scan provide information on bone quality in addition to BMD: a biomechanical ex vivo study. *Diagnostics (Basel)* 2022; 12: 3143. DOI: 10.3390/diagnostics12123143.
17. Ito K, Muraoka H, Hirahara N, Sawada E, Okada S, Kaneda T. Computed tomography texture analysis of mandibular condylar bone marrow in diabetes mellitus patients. *Oral Radiol* 2021; 37: 693-699.
18. Ito K, Muraoka H, Hirahara N, et al. Quantitative assessment of mandibular bone marrow using computed tomography texture analysis for detect stage 0 medication-related osteonecrosis of the jaw. *Eur J Radiol* 2021; 145: 110030. DOI: 10.1016/j.ejrad.2021.110030.
19. Bianchi-de Moraes M, Queiroz Costa NC, Santos da Silva GY, Calvo Costa F, Raldi FV, Pereira de Castro Lopes SL. Unveiling degenerative bone changes in the condyle: a texture analysis approach using cone-beam computed tomography. *Acta Cir Bras* 2025; 40: e401325. DOI: 10.1590/acb401325.
20. Muraoka H, Kaneda T, Ito K, Otsuka K, Tokunaga S. Early detection of acute mandibular osteomyelitis using computed tomography texture analysis. *Oral Surg Oral Med Oral Pathol Oral Radiol* 2025; 140: 634-641.
21. Drumstas Nussi A, Pereira de Castro Lopes SL, De Rosa CS, Perez Gomes JP, Ogawa CM, Braz-Silva PH, Ferreira Costa AL. In vivo study of cone beam computed tomography texture analysis of mandibular condyle and its correlation with gender and age. *Oral Radiol* 2023; 39: 191-197.
22. Bayat N, Ghavimi MA, Rahimipour K, Razi S, Esmaeili F. Radiographic texture analysis of the hard tissue changes following socket preservation with allograft and xenograft materials for dental implantation: a randomized clinical trial. *Oral Maxillofac Surg* 2024; 28: 705-713.
23. An CH, An SY, Choi BR, Huh KH, Heo MS, Yi WJ, et al. Hard and soft tissue changes of osteomyelitis of the jaws on CT images. *Oral Surg Oral Med Oral Pathol Oral Radiol* 2012; 114: 118-126.
24. Song M, Sun J, Lv K, Li J, Shi J, Xu Y. A comprehensive review of pathology and treatment of staphylococcus aureus osteomyelitis. *Clin Exp Med* 2025; 25: 131. DOI: 10.1007/s10238-025-01595-1.
25. Pugmire BS, Shailam R, Gee MS. Role of MRI in the diagnosis and treatment of osteomyelitis in pediatric patients. *World J Radiol* 2014; 6: 530-537.
26. Dobaria DG, Cohen HL. Osteomyelitis imaging. In: *StatPearls*. Treasure Island (FL): StatPearls Publishing; 2023.
27. Lee YJ, Sadigh S, Mankad K, Kapse N, Rajeswaran G. The imaging of osteomyelitis. *Quant Imaging Med Surg* 2016; 6: 184-198.
28. Muraoka H, Ito K, Hirahara N, Komatsu T, Kondo T, Kaneda T. The diagnostic utility of size and apparent diffusion coefficient values for cervical lymph nodes in patients with osteomyelitis of the jaw bone. *Oral Radiol* 2022; 38: 192-198.